Journal of Materials Chemistry A

PAPER

View Article Online
View Journal | View Issue

Cite this: *J. Mater. Chem. A*, 2015, **3**, 22274

Large active layer thickness toleration of high-efficiency small molecule solar cells†

Qian Zhang,[a] Bin Kan,[a] Xiangjian Wan,*[a] Hua Zhang,[b] Feng Liu,[c] Miaomiao Li,[a] Xuan Yang,[a] Yunchuang Wang,[a] Wang Ni,[a] Thomas P. Russell,[d] Yan Shen*[b] and Yongsheng Chen*[a]

High-efficiency organic solar cells with large active layer thickness toleration are in high demand to meet the challenges in feasible commercial production on a large scale. Generally, devices with thick active layers are preferred because they allow both the formation of a more uniform film and the effective utilization of incident light. In this work, solar cell devices with layer thicknesses ranging from 65 to 370 nm based on a small molecule donor DR3TSBDT and electron acceptor $PC_{71}BM$ were fabricated and the thickness dependence of the photovoltaic performance was systematically studied. High power conversion efficiencies (PCEs) were well-maintained in a wide layer thickness range, and for devices with layer thicknesses of 280 and 370 nm, PCEs that were off by only ∼8% and 20%, respectively, from the best PCE value of 9.95% at 120 nm were achieved. With systematic investigations, the well-maintained high performance is attributed to the fact that both the nearly ideal morphology (a bi-continuous interpenetrating crystalline nano-fibrillar structure) of the active layer and the hole mobility remained largely unchanged over the wide thickness range. Also as expected, with increasing thickness, larger transport resistance, charge recombination and transit times were observed, which made the fill factor lower. But these inferior factors were largely compensated by the increased current, and thus well-maintained high performance was achieved.

Received 23rd August 2015
Accepted 22nd September 2015

DOI: 10.1039/c5ta06627a

www.rsc.org/MaterialsA

Published on 22 September 2015. Downloaded by Nankai University on 15/11/2015 05:50:55.

Due to the rapid development in the last few years, the power conversion efficiencies (PCEs) of organic solar cells (OSCs) have increased to over 10%,[1–14] but one of the remaining challenges for high-throughput production is to develop materials and devices which can tolerate large active layer thickness variations. Accurate thickness control, if not impossible at the industrial scale, would dramatically increase the capital investment and thus processing cost. Thick active layers are preferred because it is easy to form uniform films with lower defect densities (pinholes) and enhance the reproducibility of OSCs.[15,16] In addition, increasing the active layer thickness can also realize a more effective utilization of incident light. However, the majority of reported devices so far based on both polymers and small molecules with high PCEs typically had thin active layers of ∼100 nm, and most of the device performances were also sensitive to the active layer thickness.[1,4–6,17–20] Generally, an active layer thickness of over 200 nm is a prerequisite in view of the feasibility and cost issues in future large scale printing processes.[16,21]

To the best of our knowledge, only a few reports studied the active layer thickness dependence of the photovoltaic performance, especially with thicknesses above 300 nm.[22–32] In addition, there is no report about the issue based on solution processed small molecule based devices. In this work, using one of the best reported small molecule donors, DR3TSBDT,[33] devices with a series of active layer thicknesses in the range of 65–370 nm were fabricated and the thickness dependence of the photovoltaic performance was systematically studied. High power conversion efficiencies (PCEs) were maintained over a wide range of active layer thicknesses. PCEs of 9.15% and 7.93% were achieved with active layer thicknesses of 280 and 370 nm, which were only ∼8% and 20%, respectively, from the best PCE value of 9.95% at the active layer thickness of 120 nm. Systematic morphological characterization studies indicate that all active layers with various thicknesses possessed similar morphologies with optimal highly ordered nano-fibrillar structures, which is beneficial for the efficient exciton dissociation

[a]State Key Laboratory and Institute of Elemento-Organic Chemistry and Centre for Nanoscale Science and Technology, Institute of Polymer Chemistry and Collaborative Innovation Center of Chemical Science and Engineering (Tianjin), College of Chemistry, Nankai University, Tianjin 300071, China

[b]Wuhan National Laboratory for Optoelectronics, School of Optical and Electronic Information, Huazhong University of Science and Technology, Wuhan, Hubei 430074, China

[c]Materials Science Divisions, Lawrence Berkeley National Lab, Berkeley 94720, USA

[d]Department of Polymer Science and Engineering, University of Massachusetts, Amherst 01003, USA

† Electronic supplementary information (ESI) available: Materials, characterizations, instruments, Fig. S1–S8 and Tables S1–S4. See DOI: 10.1039/c5ta06627a

This journal is © The Royal Society of Chemistry 2015

Published on 22 September 2015. Downloaded by Nankai University on 15/11/2015 05:50:55.

and charge transport. Furthermore, there were nearly no changes in the device hole mobilities when the active layer thickness increased. And with increasing active layer thickness, the transport resistance, charge recombination and transit time increased, which made the fill factor (FF) lower. But the reduction in the FF was largely offset by the increased current resulting from the increased overall light absorption, and thus well-retained high performance for thick devices was observed.

Devices based on the blend system of DR3TSBDT and [6,6]-phenyl-C_{71} butyric acid methyl ester ($PC_{71}BM$) with different active layer thicknesses were fabricated using similar procedures to those that we have reported.[33] The concentrations of the mixtures of DR3TSBDT and $PC_{71}BM$ and the spin-coating speeds were varied to form different active layer thicknesses. The average solar cell parameters with active layer thicknesses varying from 65–370 nm are summarized in Table 1. The typical current density–voltage (J–V) characteristic curves for devices with active layer thicknesses of 120, 230, 280 and 320 nm are shown in Fig. 1a. As shown in Table 1 and Fig. 1b, the V_{oc} of the devices with different active layer thicknesses remained nearly unchanged with values from 0.87 to 0.91 V. Meanwhile, the J_{sc} of the devices initially increased with increasing active layer thickness resulting from the increased absorption, then decreased due to the optical interference, and then remained nearly constant while further increasing the active layer thickness. This is consistent with the optical simulation results calculated using transfer-matrix methods (TMM) as demonstrated in Fig. 1b, which reveals that the first interference minimum is at thickness of 180 nm and the optical absorption becomes nearly impervious to the destructive interference when the active layer thickness is >200 nm. Fig. 1c shows the external quantum efficiency (EQE) spectra for the devices with different active layer thicknesses. The device with a 65 nm thick active layer exhibited a low EQE of 47% at 580 nm. And a high EQE of 69% at 580 nm was achieved when the active layer thickness increased to 90 nm. With a further increase in the thickness in the range of 120 to 370 nm, the devices displayed an almost relatively flat EQE of over 70% between 350 and 700 nm. The integrated current density from the EQE spectra is consistent with the measured J_{sc} within a 5% deviation. From Fig. 1d, the FF decreased with the increase of the active layer thickness. The decreased FF for thick active layers was attributed to the

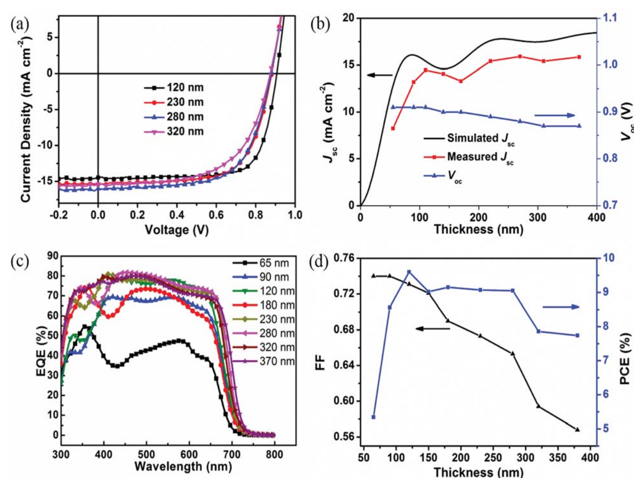

Fig. 1 (a) Current density *versus* voltage (J–V) characteristics for DR3TSBDT:$PC_{71}BM$ devices with 120, 230, 280 and 320 nm thick active layers. (b) Variation in the simulated (black line) and measured J_{sc} (red line) and the V_{oc} (blue line) with active layer thicknesses in the range of 65–370 nm. (c) Corresponding EQE spectra for the devices. (d) Average FF and PCE *versus* active layer thickness for the devices.

improved transport resistance, charge accumulation and transit time with increasing active layer thicknesses, which will be discussed below. However, the reduction of the FF was largely compensated by the increased J_{sc}, and thus high performances were well-maintained for thick active layer devices. From Fig. 1d, high PCEs of 9.15% and 7.97% were retained with active layer thicknesses of 280 and 370 nm, respectively. Note that these are within 8% and 20%, respectively, of the best performance for the device with a active layer thickness of 120 nm.

The thickness dependence of the FF is closely associated with the electrical property variations in the devices, which were systematically investigated using impedance spectroscopy (IS)[34,35] under 20 mW cm^{-2} illumination intensity using a white light emitting diode. Representative impedance data, in the form of Nyquist curves for devices with different active layer thicknesses measured at different biases close to the V_{oc} are shown in Fig. S3.† IS data were modelled using the equivalent circuit (shown in the inset Fig. S3a†) to identify physical parameters: a series resistance R_s, a transport resistance R_1, a

Table 1 The average photovoltaic parameters for DR3TSBDT:$PC_{71}BM$ devices with active layer thicknesses varying from 65–370 nm under AM 1.5 G solar illumination. The best PCEs are provided in parentheses

Thickness (nm)	V_{oc} (V)	J_{sc} (mA cm^{-2})	$J_{sc,EQE}$ (mA cm^{-2})	FF (%)	PCE (%)
65	0.91 ± 0.01	8.23 ± 0.20	7.86	74.0 ± 0.2	5.34(5.55)
90	0.91 ± 0.01	13.17 ± 0.22	12.57	74.0 ± 0.1	8.56(8.88)
120	0.91 ± 0.01	14.45 ± 0.18	14.10	73.1 ± 0.3	9.60(9.95)
150	0.90 ± 0.01	14.00 ± 0.23	13.35	72.1 ± 0.3	9.02(9.13)
180	0.90 ± 0.01	13.20 ± 0.15	12.73	69.0 ± 0.2	8.15(8.26)
230	0.89 ± 0.01	15.22 ± 0.25	14.69	67.3 ± 0.2	9.07(9.20)
280	0.88 ± 0.01	15.82 ± 0.15	15.23	65.3 ± 0.3	9.05(9.15)
320	0.87 ± 0.01	15.21 ± 0.23	14.68	59.4 ± 0.5	7.86(8.15)
370	0.87 ± 0.01	15.66 ± 0.20	15.11	56.8 ± 0.3	7.74(7.97)

Published on 22 September 2015. Downloaded by Nankai University on 15/11/2015 05:50:55.

constant phase element (CPE_1) associated with the depletion region within the active layer, and a recombination resistance R_{rec} in parallel with a CPE_2.[36] A CPE represents a non-ideal capacitor which includes an adjustable parameter to compensate for the non-homogeneity of the blocking interface (surface states, *etc.*) when put in parallel with a resistor. The capacitance for a CPE is calculated using the equation $C_\mu = (Y_0R)^{\frac{1}{n}}/R$, where Y_0 and n are the two parameters of the CPE obtained from the equivalent circuit fitting. The R_s represents the resistive losses in the ITO and PEDOT:PSS. The R_1/CPE_1 combination contributes to the high frequency response in the Nyquist plot, which is related to the information about the electronic transport in bulk as well as the dielectric contributions. The R_{rec}/CPE_2 arc contributes to the low frequency response, which is associated with the charge carrier recombination process in the active layer. The fitting parameters are demonstrated in the ESI.† First, the transport resistance R_1 improved with the increase in the layer thickness as shown in Fig. 2a. Second, from Fig. 2c, with increasing layer thickness, the capacitance C_μ obtained from the low frequency regime increased, indicating more carrier accumulation inside the active layer.[37] Physically, the accumulated photo-generated carriers that increase C_μ have two ways to escape: they are either collected through the external pathway or recombined through the recombination resistor (R_{rec}). So a decreased R_{rec} represents a higher probability of carrier recombination with increasing layer thickness (Fig. 2b). The recombination lifetime is a product of C_μ and R_{rec}. Fig. S4b† presents the electron lifetime as a function of the charge density for devices with different active layer thicknesses. At a given charge density, the device with a 120 nm-thick film showed the longest electron lifetime. A shorter electron lifetime was observed for the devices with thicker active layers (Fig. S4b†), indicating that the accumulated charge in the active layer plays an important role on the interfacial charge recombination process. This result agrees well with the observation of V_{oc} and FF for various devices, which decrease as the active layer thickness increases.

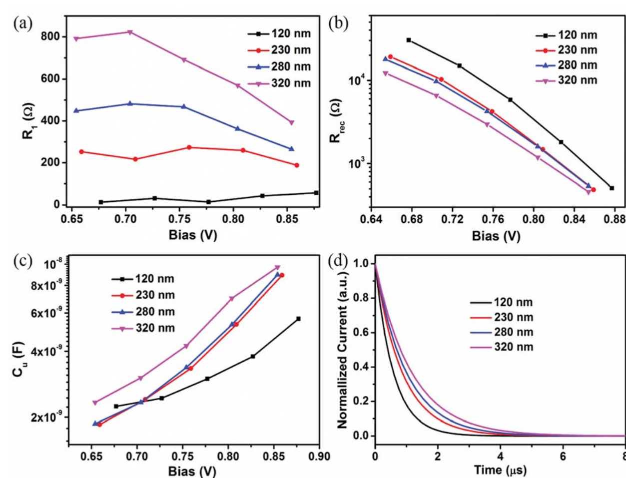

Fig. 2 (a) The transport resistance R_1, (b) recombination resistance R_{rec} and (c) chemical capacitance C_μ as a function of different biases close to the open circuit voltage obtained from electrochemical impedance spectroscopy. (d) Comparison of the normalized short-circuit current dynamics of DR3TSBDT:$PC_{71}BM$ cells with 120, 230, 280 and 320 nm-thick active layers.

The dynamics dependent on the active layer thickness for the DR3TSBDT:$PC_{71}BM$ devices were also studied using transient photocurrent (TPC)[38] measurements at the short circuit condition under 1 ms step pulse illumination. Fig. 2d presents the normalized photocurrent transients with increasing active layer thickness. The transit time is shown in Table S5.† It clearly shows that the photocurrent dynamics systematically become slower with increasing thickness, suggesting longer extraction times and an increase in the distance carriers need to traverse.[39]

In order to further understand the reduction of the FF with an increase in the active layer thickness, the relationships between the photocurrent density (J_{ph}) and the effective voltage (V_{eff}) or light intensity (P_{in}) for the devices with different active layer thicknesses were studied. The normalized photocurrent–effective voltage (J_{ph}–V_{eff}) curves for the DR3TSBDT:$PC_{71}BM$ devices with 120, 230, 280 and 320 nm-thick active layers are shown in Fig. 3a. The photocurrent is defined as $J_{ph} = J_L - J_D$, where J_L and J_D are the current densities under illumination and in the dark, respectively. $V_{eff} = V_o - V_a$, where V_o is the voltage at which $J_{ph} = 0$ and V_a is the applied voltage. The curves for all three devices with thicknesses of 120, 230 and 280 nm look very similar despite the increase in the active layer thickness. When $V_{eff} > 0.20$ V, the photocurrent of the three devices saturated with increasing voltage. In this saturation regime, the internal field was strong enough to separate excitons and efficiently extract photo-generated carriers. The voltage corresponding to the short circuit conditions (about 0.89 V) fell in the saturation regime (J_{sat}), indicative of efficient exciton dissociation and charge collection. These results correlate well with the high FFs of 65% to 73% obtained for the above three devices. However, when the active layer thickness increased to 320 nm, a square root effective voltage dependence on J_{ph} was observed (as shown by the solid line in Fig. 3a). The origin of such a square root dependence of the photocurrent was explained by Goodman and Rose in 1971, and is an indication of either recombination-

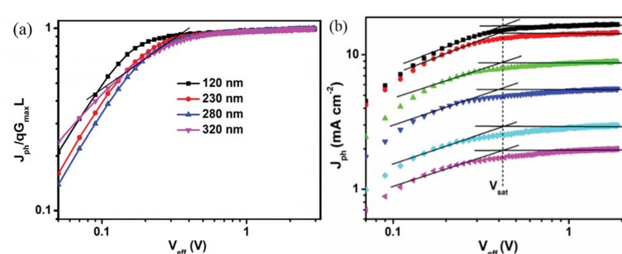

Fig. 3 (a) Effective photocurrent density (J_{ph}) normalized by J_{sat} as a function of effective voltage (V_{eff}) under 100 mW cm^{-2} illumination for DR3TSBDT:$PC_{71}BM$ cells with 120, 230, 280 and 320 nm-thick active layers (the solid black line indicates a square root dependence). (b) J_{ph} of a 320 nm-thick DR3TSBDT:$PC_{71}BM$ cell *versus* V_{eff} at different intensities (10 to 100 mW cm^{-2}). Solid lines indicate square root and saturation regimes as a guide for the eye where V_{sat} indicates the saturation voltage.

This journal is © The Royal Society of Chemistry 2015

Published on 22 September 2015. Downloaded by Nankai University on 15/11/2015 05:50:55.

limited (eqn (1)) or space-charge-limited (SCL) photocurrent (eqn (2)):[40]

$$J_{\mathrm{ph}} = qG\sqrt{\mu_{\mathrm{h(e)}}\tau_{\mathrm{h(e)}}}\sqrt{V} \quad (1)$$

$$J_{\mathrm{ph}} \leq (qG)^{0.75}\left(\frac{9}{8}\varepsilon_0\varepsilon_{\mathrm{r}}\varepsilon_{\mathrm{h}}\right)^{0.25}\sqrt{V} \quad (2)$$

where G is the generation rate of free charge carriers.

For the former case, a low mobility or short lifetime of the free carriers, due to recombination or trapping, leads to the mean electron or hole (or both) drift length becoming smaller than the active layer thickness and thus recombination of charge carriers becomes considerable.[41,42] For the latter case, at high light intensities the build-up of space charges (which is the origin of the non-uniform electric field) reaches a fundamental limit.[43] Analysing the light intensity dependence of the photocurrent and the point at which the square root regime forms a transition into the saturation regime V_{sat} is an effective method to distinguish between these two physically distinct cases. While in the first (recombination-limited) case the photocurrent scales linearly with the light intensity, SCL photocurrent scales with a three-fourth power law dependence. Besides, V_{sat} is either independent of the light intensity (recombination-limited) or scales with a one half power of the light intensity (SCL case).[41]

The photocurrent of a 320 nm-thick DR3TSBDT:$PC_{71}BM$ solar cell *versus* V_{eff} at different intensities is shown in Fig. 3b. Neutral density filters were used to control the incident light intensity, which was varied from 10 to 100 mW cm^{-2}. It is clear that V_{sat} does not change with decreasing light intensity, as expected for a recombination-limited photocurrent. Furthermore, for the solar cell with a 320 nm-thick active layer, J_{ph} showed a sub-linear dependence on the light intensity with a linear fit with a slope of 0.902 at the maximum power-output point (Fig. S5†), which could also be a sign of significant bimolecular recombination.[44] Therefore, the photocurrent observed for the DR3TSBDT:$PC_{71}BM$ devices clearly showed the fingerprints of a recombination-limited photocurrent.[41] This may be due to the relatively low mobility of 6.13×10^{-4} cm^2 V^{-1} s^{-1} compared with that of the reported polymers.[22,29] So a higher rate of forming photo-generated charge carriers in thick devices resulted in more charge accumulation and bimolecular recombination, which was consistent with its relatively larger transport resistance and chemical capacitance as discussed above. Thus, the photovoltaic performance for the 320 nm-thick devices was sharply reduced.

The morphology of the active layers can be a determining factor for the well-maintained high photovoltaic performance. The nanoscale morphologies of the DR3TSBDT:$PC_{71}BM$ blends with different thicknesses were measured using atomic force microscopy (AFM) and high-resolution transmission electron microscopy (HR-TEM). From the AFM images (Fig. S6†), all films with different thicknesses exhibited a bi-continuous interpenetrating network and a small root-mean-square (RMS) roughness of about 1 nm, which indicated that these films were smooth and uniform. From the TEM images (Fig. 4), no particularly different morphologies such as large size aggregations of nanoparticles were found for thick active layers. And well-distributed nano-fibrillar structures with a bi-continuous interpenetrating network could be observed, which are favourable for exciton dissociation and charge transport, and thus high values of J_{sc} and FF.

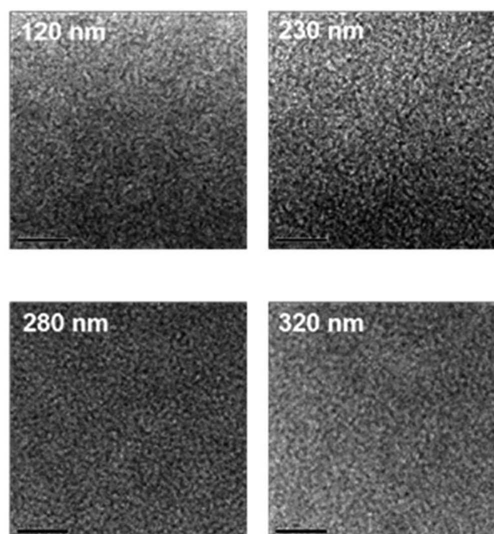

Fig. 4 TEM images of DR3TSBDT:$PC_{71}BM$ with different active layer thicknesses. The scale bar is 200 nm.

To further understand the microstructures of the active layers with different thicknesses, grazing incidence X-ray diffraction (GIXD) was measured (Fig. 5). The line-cuts of all the diffractions are shown in Fig. S7.† All films show multiple higher order (*h*00) reflections, indicative of a long-range order and lateral packing of the backbones. In addition, the strong reflection of the (010) peaks characteristic of the π–π stacking distance (3.61 Å), shows a large azimuthal distribution for all films, which suggests the mixture of face-on and edge-on packing. Similar pattern behaviour in the GIXDs indicates that

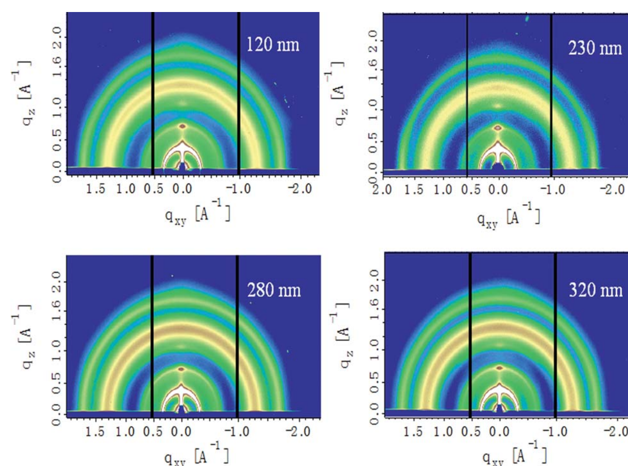

Fig. 5 The GIXD profiles of DR3TSBDT:$PC_{71}BM$ films with different thicknesses.

Published on 22 September 2015. Downloaded by Nankai University on 15/11/2015 05:50:55.

DR3TSBDT possesses the same ordered structure in the blend composition for a wide range of thicknesses. Thus, all films with various thicknesses exhibited similar morphologies with highly ordered nano-fibrillar structures, which are beneficial for efficient exciton diffusion and dissociation and charge transport. Additionally, hole mobility for different thickness-devices were measured using the space-charged-limited-current (SCLC) method. Notably, the magnitude of the hole mobility of DR3TSBDT remained the same for all active layer thicknesses from 120 nm to 370 nm and showed negligible changes with a value of 3.20×10^{-4} cm^2 V^{-1} s^{-1} for the 370 nm-thick film (Fig. S8†). These morphology and SCLC results are consistent with the maintained high performance of the thick devices.

Conclusion

To conclude, devices with a series of active layer thicknesses in the range of 65–370 nm based on the small molecule donor, DR3TSBDT, were fabricated and the thickness dependence of the photovoltaic performance, mechanisms and morphology was systematically investigated. All active layers with various thicknesses possessed similar morphologies with highly ordered nano-fibrillar structures, which are beneficial for efficient exciton dissociation and charge transport. And the hole mobility hardly changed as the active layer thickness increased. Thick active layers enabled more light absorption, yielding a high J_{sc} of ~15.92 mA cm^{-2}. Nevertheless, with the increase in active layer thickness, the transport resistance, charge accumulation and the distance carriers needed to traverse increased, thus leading to more bimolecular recombination and a decreased FF. However, the inferior factor of FF reduction was largely compensated by the increased absorption, and thus high PCEs of 9.15% were achieved with an active layer thickness of 280 nm. And devices with active layer thicknesses of 370 nm retained 80% of the best PCE achieved at a thickness of 120 nm. The high efficiency for the thick active layers and the high toleration of active layer thickness variations make DR3TSBDT:PC$_{71}$BM films promising candidates for low-cost, high-throughput industry photovoltaic applications.

Acknowledgements

The authors gratefully acknowledge the financial support from MoST (2014CB643502), NSFC (51373078, 51422304, 91433101), PCSIRT (IRT1257) and Tianjin city (13RCGFGX01121).

Notes and references

1 Z. He, B. Xiao, F. Liu, H. Wu, Y. Yang, S. Xiao, C. Wang, T. P. Russell and Y. Cao, *Nat. Photonics*, 2015, **9**, 174.
2 Y. Liu, J. Zhao, Z. Li, C. Mu, W. Ma, H. Hu, K. Jiang, H. Lin, H. Ade and H. Yan, *Nat. Commun.*, 2014, **5**, 5293.
3 B. Kan, M. Li, Q. Zhang, F. Liu, X. Wan, Y. Wang, W. Ni, G. Long, X. Yang, H. Feng, Y. Zuo, M. Zhang, F. Huang, Y. Cao, T. P. Russell and Y. Chen, *J. Am. Chem. Soc.*, 2015, **137**, 3886.
4 C. Liu, C. Yi, K. Wang, Y. Yang, R. S. Bhatta, M. Tsige, S. Xiao and X. Gong, *ACS Appl. Mater. Interfaces*, 2015, **7**, 4928.
5 L. Ye, S. Zhang, W. Zhao, H. Yao and J. Hou, *Chem. Mater.*, 2014, **26**, 3603.
6 L. K. Jagadamma, M. Al-Senani, A. El-Labban, I. Gereige, G. O. Ngongang Ndjawa, J. C. D. Faria, T. Kim, K. Zhao, F. Cruciani, D. H. Anjum, M. A. McLachlan, P. M. Beaujuge and A. Amassian, *Adv. Energy Mater.*, 2015, **5**, 1500204.
7 L. Zuo, C. Chang, C. Chueh, S. Zhang, H. Li, A. K. Y. Jen and H. Chen, *Energy Environ. Sci.*, 2015, **8**, 1712.
8 L. Huo, T. Liu, X. Sun, Y. Cai, A. J. Heeger and Y. Sun, *Adv. Mater.*, 2015, **27**, 2938.
9 S. Zhang, L. Ye, W. Zhao, B. Yang, Q. Wang and J. Hou, *Sci. China: Chem.*, 2015, **58**, 248.
10 J. Chen, C. Cui, Y. Le, L. Zhou, Q. Ou, C. Li, Y. Li and J. Tang, *Adv. Mater.*, 2015, **27**, 1035.
11 L. Nian, W. Zhang, N. Zhu, L. Liu, Z. Xie, H. Wu, F. Wurthner and Y. Ma, *J. Am. Chem. Soc.*, 2015, **137**, 6995.
12 Y. Liu, C. Chen, Z. Hong, J. Gao, Y. Yang, H. Zhou, L. Dou, G. Li and Y. Yang, *Sci. Rep.*, 2013, **3**, 3356.
13 H. Zhou, Y. Zhang, C. Mai, S. D. Collins, G. C. Bazan, T. Q. Nguyen and A. J. Heeger, *Adv. Mater.*, 2015, **27**, 1767.
14 A. R. M. Yusoff, D. Kim, H. P. Kim, F. K. Shneider, W. J. Silva and J. Jang, *Energy Environ. Sci.*, 2015, **8**, 303.
15 P. W. M. Blom, V. D. Mihailetchi, L. J. A. Koster and D. E. Markov, *Adv. Mater.*, 2007, **19**, 1551.
16 T. D. Nielsen, C. Cruickshank, S. Foged, J. Thorsen and F. C. Krebs, *Sol. Energy Mater. Sol. Cells*, 2010, **94**, 1553.
17 Z. He, C. Zhong, S. Su, M. Xu, H. Wu and Y. Cao, *Nat. Photonics*, 2012, **6**, 591.
18 Q. Zhang, B. Kan, F. Liu, G. Long, X. Wan, X. Chen, Y. Zuo, W. Ni, H. Zhang, M. Li, Z. Hu, F. Huang, Y. Cao, Z. Liang, M. Zhang, T. P. Russell and Y. Chen, *Nat. Photonics*, 2015, **9**, 35.
19 L. Lu, W. Chen, T. Xu and L. Yu, *Nat. Commun.*, 2015, **6**, 7327.
20 C. Li, C. Chang, Y. Zang, H.-X. Ju, C.-C. Chueh, P.-W. Liang, N. Cho, D. S. Ginger and A. K. Y. Jen, *Adv. Mater.*, 2014, **26**, 6262.
21 F. C. Krebs, *Sol. Energy Mater. Sol. Cells*, 2009, **93**, 1636.
22 W. Li, K. H. Hendriks, W. S. C. Roelofs, Y. Kim, M. M. Wienk and R. A. J. Janssen, *Adv. Mater.*, 2013, **25**, 3182.
23 S. C. Price, A. C. Stuart, L. Yang, H. Zhou and W. You, *J. Am. Chem. Soc.*, 2011, **133**, 4625.
24 Y. Zhang, J. Liu, L. Zhang, J. Fang, W. Zhang and Z. Liu, *Chin. J. Org. Chem.*, 2014, **34**, 1021.
25 C. E. Small, S. W. Tsang, S. Chen, S. Baek, C. M. Amb, J. Subbiah, J. R. Reynolds and F. So, *Adv. Energy Mater.*, 2013, **3**, 909.
26 Z. Lu, B. Jiang, X. Zhang, A. Tang, L. Chen, C. Zhan and J. Yao, *Chem. Mater.*, 2014, **26**, 2907.
27 R. Kroon, A. Diaz de Zerio Mendaza, S. Himmelberger, J. Bergqvist, O. Bäcke, G. C. Faria, F. Gao, A. Obaid, W. Zhuang, D. Gedefaw, E. Olsson, O. Inganäs, A. Salleo, C. Müller and M. R. Andersson, *J. Am. Chem. Soc.*, 2014, **136**, 11578.
28 S. Lee, S. Nam, H. Kim and Y. Kim, *Appl. Phys. Lett.*, 2010, **97**, 103503.

 This journal is © The Royal Society of Chemistry 2015

29 T. L. Nguyen, H. Choi, S. J. Ko, M. A. Uddin, B. Walker, S. Yum, J. E. Jeong, M. H. Yun, T. J. Shin, S. Hwang, J. Y. Kim and H. Y. Woo, *Energy Environ. Sci.*, 2014, **7**, 3040.
30 K. Sun, Z. Xiao, S. Lu, W. Zajaczkowski, W. Pisula, E. Hanssen, J. M. White, R. M. Williamson, J. Subbiah, J. Ouyang, A. B. Holmes, W. W. H. Wong and D. J. Jones, *Nat. Commun.*, 2015, **6**, 6013.
31 H. Choi, S.-J. Ko, T. Kim, P.-O. Morin, B. Walker, B. H. Lee, M. Leclerc, J. Y. Kim and A. J. Heeger, *Adv. Mater.*, 2015, **27**, 3318.
32 V. Vohra, K. Kawashima, T. Kakara, T. Koganezawa, I. Osaka, K. Takimiya and H. Murata, *Nat. Photonics*, 2015, **9**, 403.
33 B. Kan, Q. Zhang, M. Li, X. Wan, W. Ni, G. Long, Y. Wang, X. Yang, H. Feng and Y. Chen, *J. Am. Chem. Soc.*, 2014, **136**, 15529.
34 G. Garcia-Belmonte, P. P. Boix, J. Bisquert, M. Sessolo and H. J. Bolink, *Sol. Energy Mater. Sol. Cells*, 2010, **94**, 366.
35 G. Garcia-Belmonte, A. Munar, E. M. Barea, J. Bisquert, I. Ugarte and R. Pacios, *Org. Electron.*, 2008, **9**, 847.
36 G.-H. Kim, H.-K. Song and J. Y. Kim, *Sol. Energy Mater. Sol. Cells*, 2011, **95**, 1119.
37 G. Perrier, R. de Bettignies, S. Berson, N. Lemaitre and S. Guillerez, *Sol. Energy Mater. Sol. Cells*, 2012, **101**, 210.
38 C. G. Shuttle, A. Maurano, R. Hamilton, B. O'Regan, J. C. de Mello and J. R. Durrant, *Appl. Phys. Lett.*, 2008, **93**, 183501.
39 Z. Li, F. Gao, N. C. Greenham and C. R. McNeill, *Adv. Funct. Mater.*, 2011, **21**, 1419.
40 A. M. Goodman and A. Rose, *J. Appl. Phys.*, 1971, **42**, 2823.
41 M. Lenes, M. Morana, C. J. Brabec and P. W. M. Blom, *Adv. Funct. Mater.*, 2009, **19**, 1106.
42 K. R. Choudhury, J. Subbiah, S. Chen, P. M. Beaujuge, C. M. Amb, J. R. Reynolds and F. So, *Sol. Energy Mater. Sol. Cells*, 2011, **95**, 2502.
43 V. D. Mihailetchi, J. Wildeman and P. W. M. Blom, *Phys. Rev. Lett.*, 2005, **94**, 126602.
44 C. M. Proctor, C. Kim, D. Neher and T.-Q. Nguyen, *Adv. Funct. Mater.*, 2013, **23**, 3584.

Published on 22 September 2015. Downloaded by Nankai University on 15/11/2015 05:50:55.

This journal is © The Royal Society of Chemistry 2015